Mecánica Computacional Vol. XXI, pp. 237–255
S. R. Idelsohn, V. E. Sonzogni and A. Cardona (Eds.)
Santa Fe–Paraná, Argentina, October 2002

NUMERICAL SIMULATION OF TIME-DEPENDENT REACTING FLOWS

José P. Tamagno[+], Sergio A. Elaskar[+] and Gustavo A. Ríos*

+ Departamento de Aeronáutica, Universidad Nacional de Córdoba
Av. Velez Sarfield 1601, Córdoba (5000), Argentina
e-mail: jtamagno@efn.uncor.edu – selaskar@efn.uncor.edu

* Instituto Universitario Aeronáutico
Ruta 20, km 5.5, Córdoba (5022), Argentina
e-mail: gusadrr@yahoo.com.ar

Abstract. *A numerical methodology for solving quasi-one dimensional, time-dependent reacting flow problems is outlined in this paper. The numerical approach uses a finite-volume Harten-Yee TVD scheme for the Euler equations of motion coupled with finite rate chemistry. Gas interfaces are detected and tracked via a Riemann solver and to reduce the number of nodes without smearing the interfaces, a moving mesh is used. The source terms representing the finite-rate chemical kinetics and vibrational relaxation are often large and make the algorithm too stiff to be advanced explicitly. To avoid this stiffness an implicit treatment of these source terms is implemented. The numerical program can work with 13 chemical reacting species and 33 different reactions of a hydrogen-oxygen-nitrogen combustion mechanism, each of which may proceed forward or backward. Since helium is often employed in certain applications it has also been included, although, it was considered an inert species. Numerical simulations that show the potential of the computer code in predicting flow properties, wave patterns and chemical compositions are presented.*

Resumen. *Se presenta una técnica numérica para solucionar problemas cuasi unidimensionales no estacionarios, en los cuales el flujo es químicamente activo. La solución de las ecuaciones de Euler a las cuales se han acoplado reacciones químicas finitas, se consigue aplicando un esquema TVD de Harten-Yee. Las interfaces entre distintos gases son detectadas con una técnica tipo "solver" de Riemann y se utiliza una malla móvil para disminuir la cantidad de nodos y evitar la difusión numérica de dichas interfaces. Debido a la dependencia exponencial con la temperatura, los términos fuentes que resultan de la cinética de las reacciones químicas pueden llegar a ser de gran magnitud. Esto hace que el conjunto de las ecuaciones de las especies sea "stiff" y tenga que utilizarse un procedimiento implícito. El programa de cálculo numérico puede trabajar con 13 especies reactivas y 33 reacciones químicas que describen el mecanismo de la combustión hidrógeno-oxígeno-nitrógeno. Por ser el gas Helio utilizado en muchas aplicaciones también ha sido incluido, aunque se lo considere una especie inerte. Se presentan resultados de algunas simulaciones numéricas, las cuales fueron realizadas con el propósito de mostrar el potencial del código de cómputos para predecir propiedades del flujo, configuraciones de ondas y composición química.*

1 INTRODUCTION

There are many interesting unsteady flow problems in which the fluid dynamics governing equations are the quasi one-dimensional Euler's equations with source terms to account for chemical and vibrational non-equilibrium, viscous and heat-conduction losses. Expansion and shock tube flows belong to this class of problems. These particular flows are very demanding test cases for any unsteady one-dimensional code. In fact, such a code besides describing the type of flow generated inside the tube and of predicting correctly the wave pattern, has to be able to determine the chemical composition of the working fluid. A numerical technique, here is presented which, supposedly, can accomplish all this.

The numerical approach taken to solve the equations is based on an implicit finite-volume form of the Harten and Yee TVD scheme used to compute the bulk of the flow field[1], and on a Riemann solver used for tracking gas interfaces [2, 3]. Both techniques are applied in a moving mesh. The computer program in its current version allows the incorporation of 14 chemical species (N_2, O_2, H_2, NO, OH, NO_2, HNO, HO_2, H_2O, H_2O_2, N, O, H, He). Helium (He) is added as an inert species with a prescribed third body efficiency. Obviously, an air reaction mechanism is obtained setting the species containing hydrogen to negligible levels.

It is well known that the flow in expansion tubes as well as in shock tubes is characterized by shock waves and contact discontinuities, and in turn all these phenomenons are influenced by high temperature effects, chemical kinetics and viscous interactions. There is also a large disparity of length scales; for example, a facility may be several meters in length while the breaking of a thin diaphragm may take place in millimeters. One goal of this work is to investigate whether this kind of numerical approach can predict detailed flow features within large facilities that operate by rupturing diaphragms. With this overall objective in mind, some points of the physical modeling have been kept relatively simple, for instance, viscosity and heat conduction models are not as sophisticated as they might be.

Numerical results are computed for the NASA-GASL Hypulse facility at a single operating condition. In many simulations of the flow within an expansion tube, it is assumed that as soon as the primary shock arrives the thin second diaphragm breaks instantly. This is an ideal situation that never happens because it takes some time before this diaphragm, although thin, breaks. Therefore it is of interest to know how the secondary shock, the secondary contact discontinuity and particularly, the properties of the test flow are affected by delays due to the second diaphragm. The effect of this behavior on the working fluid quality with regard to species concentrations, are studied in detail, since the finite-rate chemistry capability in the present code allows the amount of dissociated species in the flow, created from such non-ideal behavior of the diaphragm, be estimated.

To conduct a shock tube simulation, the opening of the secondary diaphragm was sufficiently delayed to create a exceedingly large stagnation region of hot gas and high pressure at the end of the intermediate tube of Hypulse. The simulation of a shock tube driven by helium, shows that calculations still predict the tailored operating mode of the shock tube when real gas effects are accounted for, and the composition of the stagnant flow to be, eventually, expanded in the nozzle of a Shock Tunnel, determined. Although not yet done, incorporating the nozzle region of the facility can be simply done by including, as program input, the area changes associated with the nozzle.

Finite-rate chemistry mechanisms describing the detailed chemical kinetics of a reacting combustible mixture made with gaseous hydrogen, oxygen and nitrogen have been developed by a number of authors. In this study, however, the chemical mechanism assembled by Jachimowski [4] was adopted and incorporated into the computer code. The source terms representing the finite-rate chemical kinetics of hydrogen oxidation are often very large and make the algorithm too stiff to be treated explicitly and, therefore, an implicit treatment was implemented. The extra cost of inverting block matrices at each cell is offset by the increase in the size of the time step that this allows [5].

This work begins by presenting the mathematical formulation of the equations needed for solving time dependent, quasi one-dimensional reacting flows. In this equations, viscous and heat conduction losses are included in an approximated manner consistent with the one-dimensional approach taken. Next, the fundamental relations describing the net rates of change for the chemical components, the calculation of equilibrium constants and the rate of change of non equilibrium vibrational energy, are introduced. This is

followed by an abbreviated description of the numerical scheme. Finally, the results of numerical computations applied to expansion and shock tubes are presented.

2 GOVERNING EQUATIONS

The equations used to describe unsteady, quasi-one-dimensional reacting flows are the Euler equations with chemical and vibrational nonequilibrium source terms, and approximations for viscous and heat-conduction losses. The resulting system of equations are written in the following form:

$$\frac{\partial U}{\partial t}+\frac{1}{A}\frac{\partial (FA)}{\partial x}=M \tag{1}$$

U is the vector of state variables, F is the vector of convective flows and M is the vector that contains the sources terms. These vectors are defined as follows:

$$U=\begin{bmatrix}\rho_1\\ \rho_2\\ .\\ .\\ .\\ \rho_{14}\\ \rho u\\ E_v\\ E\end{bmatrix}\quad F=\begin{bmatrix}\rho_1 u\\ \rho_2 u\\ .\\ .\\ .\\ \rho_{14} u\\ \rho u^2+p\\ uE_v\\ u(E+p)\end{bmatrix}\quad M=\begin{bmatrix}w_1\\ w_2\\ .\\ .\\ .\\ w_{14}\\ S+F_w\\ w_v\\ Q_w\end{bmatrix} \tag{2}$$

A is the cross-section area of the duct and is a known function of the longitudinal coordinate x. The density of each one of the species is indicated by ρ_j and the overall density with $\rho=\sum_{j=1}^{14}\rho_j$. The others terms are de pressure p, the velocity component u, the vibrational energy per unit volume E_v and the total energy per unit volume E. The production or destruction of specie j through chemical reactions is represented by the source terms w_j, and the source of vibrational energy is represented by w_v. S is due to area changes and is defined by the expression:

$$S=\frac{p}{A}\frac{\partial A}{\partial x} \tag{3}$$

F_w represents the loss of momentum due to frictional effects and is written in the following form:

$$F_w=-\frac{4f}{D}\frac{\rho\, u|u|}{2} \tag{4}$$

where f is the friction coefficient, and D is the tube diameter. The losses in energy by unit of volume due to the heat transfer rate to the gas from the wall Q_w is given by:

$$Q_w=\frac{\alpha}{D}(T_w-T) \tag{5}$$

being α the heat transfer coefficient and T_w is the wall temperature. The application of these kinds of simple models to flows that have large boundary layers in relation to the tube diameter may not be valid at

all. Consequently, its applicability for the low density, high velocity flow in the acceleration section of an expansion tube is questionable.

The relationship between pressure and temperature is given by the equation of state for a mixture of thermically perfect gases:

$$p = \sum_{j=1}^{14} \frac{\rho_j}{W_j} RT \tag{6}$$

where R is the universal gas constant and W_j is the molecular weight of the specie j.

The total energy can be written as:

$$E = \sum_{j=1}^{14} \left(\rho_j c_{v_j} T\right) + \sum_{j=1}^{14} \rho_j h_j^0 + E_v + E_{el} + 0.5\rho\, u^2 \tag{7}$$

In the Eq. (7), the first term is the sum of the translational and rotational energies for unit of volume for each species (c_{v_j} is the rotational and translational specific heat), the second term expresses the chemical energy per unit volume and the last term the kinetic energy per unit volume. E_{el} is the sum of the energy in the excite electronic modes and E_v contains the sum of the vibrational energies for all the species. Following Wilson[5], the vibrational energies are calculated assuming harmonic oscillators with corrections for anharmonic effects applied to species that may be present in large mass fractions and have significant anharmonic terms (N_2, O_2, H_2, and H_2O). Electronics modes are included for only O_2, O and N. All thermodynamic data are obtained from JANAF tables[6].

3 CHEMICAL SOURCE TERMS

For a set of N_R elementary reactions involving N species, the rate equations can be written in the following general form[7]:

$$\sum_{j=1}^{N} \nu'_{ij} \cdot M_j \underset{k_{bi}}{\overset{k_{fi}}{\rightleftharpoons}} \sum_{j=1}^{N} \nu''_{ij} \cdot M_j \qquad i=1,...,N_R \tag{8}$$

where ν'_{ij} and ν''_{ij} are the stoichiometric coefficients for species j appearing as a reactant in the i $_{th}$ forward and backward reactions, respectively. M_j is the chemical symbol for species j. The reaction rate constants for the i $_{th}$ reaction (either forward or backward reaction, k_{fi} or k_{bi}) is given empirically by the Arrhenius expression[8]:

$$k_i = B_i \cdot T^{\alpha_i} \cdot \exp\left(-E_i/RT\right) \tag{9}$$

where E_i represents the activation energy, and B_i and α_i are constants.

According to Eq. (8), the rate of change of molar concentrations of species j by reaction i is:

$$\left(\dot{C}_j\right)_i = \left(\nu''_{ij} - \nu'_{ij}\right) \cdot \left(k_{fi} \prod_{m=1}^{N} C_m^{\nu'_{im}} - k_{bi} \prod_{m=1}^{N} C_m^{\nu''_{im}}\right) \qquad \left(\frac{mol}{m^3}\frac{1}{s}\right) \tag{10}$$

where C_j is the molar concentration of species j. After introducing the equilibrium constant K_{Ci} associated with the reaction i, the Eq. (10) can be written as:

$$\left(\dot{C}_j\right)_i = \left(\nu''_{ij} - \nu'_{ij}\right) \cdot k_{fi} \left(\prod_{m=1}^{N} C_m^{\nu'_{im}} - \frac{1}{K_{Ci}} \prod_{m=1}^{N} C_m^{\nu''_{im}}\right) \tag{11}$$

The total rate of change of molar concentrations of species j then is:

$$\dot{C}_j = \sum_{i=1}^{N_R} \left(\dot{C}_j \right)_i = \sum_{i=1}^{N_R} (\nu''_{ij} - \nu'_{ij}) \cdot R_i \tag{12}$$

where R_i is given by:

$$R_i = k_{fi} \left(\prod_{m=1}^{N} C_m^{\nu'_{im}} - \frac{1}{K_{Ci}} \prod_{m=1}^{N} C_m^{\nu''_{im}} \right) \tag{13}$$

and consequently, the total rate of mass productions of species *j* becomes:

$$\dot{w}_j = W_j \cdot \sum_{i=1}^{N_R} (\nu''_{ij} - \nu'_{ij}) \cdot R_i \qquad \left(\frac{Kg}{m^3} \frac{1}{s} \right) \tag{14}$$

being W_j the molecular weight of species *j*. It should be noted that the expression for the chemical reaction rate Eq. (11) is strictly valid for elementary reaction steps. If a global kinetic scheme is used, the molar concentrations may differ from their stoichiometric coefficients in order to match experimental data. Because of the wide variety of chemical time scales involved in combustion processes and exponential dependence of the source terms on temperature, the set of species equations in the system(1) may become very stiff in a certain temperature range.

3.1 Application to a reaction of Jachimowski's H_2 - Air combustion mechanism

Let us consider the reaction Nº 2 of Jachimowski's combustion mechanism:

$$H + O_2 \rightleftharpoons OH + O \tag{15}$$

in which the stoichiometric coefficients are:

$$\nu'_H = 1 \;;\; \nu''_H = 0 \;;\; \nu'_{O_2} = 1 \;;\; \nu''_{O_2} = 0$$
$$\nu'_{OH} = 0 \;;\; \nu''_{OH} = 1 \;;\; \nu'_O = 0 \;;\; \nu''_O = 1$$

The reaction process proceeding from left to the right produces OH and O while removing H and O_2. Proceeding right to the left affects the species in the opposite manner. According to Eq.(11), the rate of change of molar concentrations of species *j* then is:

$$\left(\dot{C}_j \right)_2 = \left(\nu''_{2j} - \nu'_{2j} \right) k_{f2} \left(C_H C_{O_2} - \frac{1}{K_{C_2}} C_{OH} C_O \right) \tag{16}$$

After replacing the number of moles by the density, the above equation becomes:

$$\left(\dot{C}_j \right)_2 = \left(\nu''_{2j} - \nu'_{2j} \right) k_{f2} \left(\frac{\rho_H}{W_H} \cdot \frac{\rho_{O_2}}{W_{O_2}} - \frac{1}{K_{C_2}} \frac{\rho_{OH}}{W_{OH}} \cdot \frac{\rho_{CO}}{W_{CO}} \right) \tag{17}$$

and the rate of mass production of species *j* due to reaction Nº 2 is:

$$\left(\dot{w}_j \right)_2 = \left(\nu''_{2j} - \nu'_2 \right) \cdot W_j \cdot R_2 \tag{18}$$

For each one of the species appearing in the reaction Nº 2, it can be obtained:

$$\begin{aligned}
(\dot{w}_{OH})_2 &= (1-0)\cdot W_{OH}\cdot R_2 = W_{OH}\cdot R_2 \qquad (a)\\
(\dot{w}_{H})_2 &= (0-1)\cdot W_{H}\cdot R_2 = -W_{H}\cdot R_2 \qquad (b)\\
(\dot{w}_{O})_2 &= (1-0)\cdot W_{O}\cdot R_2 = W_{O}\cdot R_2 \qquad (c)\\
(\dot{w}_{O_2})_2 &= (1-0)\cdot W_{O_2}\cdot R_2 = -W_{O_2}\cdot R_2 \qquad (d)
\end{aligned} \tag{19}$$

It is also of interest to consider the reactions Nº 6 and Nº 19 of Jachimowski's combustion mechanism. These reactions are:

$$\text{Reaction Nº 6: } H + OH + M \rightleftharpoons H_2 + M \tag{20}$$

$$\text{Reaction Nº 19: } M + H_2O_2 \rightleftharpoons OH + OH + M \tag{21}$$

where M refers to all possible third-body collision partners (i.e. all the species).

The expressions for R_6 and R_{19} are:

$$R_6 = \sum_{M=1}^{N} \frac{\rho_M}{W_M}\left(m_{6M} k_{f6} \frac{\rho_{OH}}{W_{OH}} \frac{\rho_H}{W_H} - m_{6M} k_{b6} \frac{\rho_{H_2O}}{W_{H_2O}} \right) \tag{22}$$

$$R_{19} = \sum_{M=1}^{N} \frac{\rho_M}{W_M}\left(m_{19M} k_{f19} \frac{\rho_{H_2O_2}}{W_{H_2O_2}} - m_{19M} k_{b19} \frac{\rho_{OH}}{W_{OH}} \frac{\rho_{OH}}{W_{OH}} \right) \tag{23}$$

where m_{6M} and m_{19M} are the third-body efficiency factors for reactions Nº 6 and Nº 19 respectively.

The rate of mass production of OH due to reaction Nº 6 is:

$$(\dot{w}_{OH})_6 = -W_{OH} R_6 \tag{24}$$

and the rate of mass production of OH due to reaction Nº 19 is:

$$(\dot{w}_{OH})_{19} = W_{OH} \cdot 2R_{19} \tag{25}$$

Consequently the mass production of species OH due to the above three reactions is:

$$(\dot{w}_{OH})_{2+6+19} = W_{OH} \cdot (R_2 - R_6 + 2R_{19}) \tag{26}$$

If all the reactions listed in the H_2 - Air combustion mechanism were taken into account, the complete source term for the OH species conservation equation is found to be:

$$\begin{aligned}
(\dot{w}_{OH})_{Complete} = W_{OH}(&2R_1 + R_2 + R_3 - R_4 - 2R_5 - R_6 + R_8 + 2R_{11}\\
&+ R_{13} - R_{14} + R_{17} - R_{18} + 2R_{19} - R_{24} + R_{27} - R_{28} + R_{30} + R_{31})
\end{aligned} \tag{27}$$

The complete set of source terms for Jachimowski's reaction mechanism is given in Appendix I.

3.2 Relation between the equilibrium constant and the Gibbs free energy

Consider the chemical reaction:

$$\nu_1' A_1' + \nu_2' A_2' \rightleftharpoons \nu_1'' B_1 + \nu_2'' B_2 \tag{28}$$

where the lower-case letters a_i and b_i are the stoichiometric coefficients and the capital letters A_i and B_i denote chemical elements or compounds. The quotient of partial pressures for this reaction is here defined as:

$$K_p = \frac{\left(p_{B_1}\right)^{\nu_1''} \cdot \left(p_{B_2}\right)^{\nu_2''}}{\left(p_{A_1}\right)^{\nu_1'} \cdot \left(p_{A_1}\right)^{\nu_2'}} \tag{29}$$

When each partial pressure in Eq. (29) is that which would exist in the thermodynamic equilibrium for reaction equation (28), then Eq. (29) gives the equilibrium constant.

If a reversible constant temperature process begins in a thermodynamic state at pressure p^e and ends in a thermodynamic state at pressure p^0 , the change in Gibbs free energy accompanying that process will satisfy the equation:

$$G^0 - G^e = RT \ln \frac{p^0}{p^e} \tag{30}$$

Now for the chemical reaction given by Eq. (28), and making use of Eq. (29), it can be obtained:

$$\Delta G^0 - \Delta G^e = RT\left(\ln K_p^0 - \ln K_p^e\right) \tag{31}$$

where K_p is defined by Eq. (29). Now, let us assume that the thermodynamic state denoted by the superscript 0 is the condition where

$$p_{A_1}^0 = p_{A_2}^0 = p_{B_1}^0 = p_{B_2}^0 = 1atm \tag{32}$$

Furthermore, identify the thermodynamic state denoted by the superscript *e* as the state of thermodynamic equilibrium at the given temperature. Then from Eq. (29),

$$K_p^0 = 1 \tag{33}$$

and according to the criterion for the existence of a state of equilibrium in a system, that the change of free energy is zero for any reversible change of that system,

$$\Delta G^e = 0 \tag{34}$$

and so Eq. (35) becomes:

$$\Delta G^0 = -RT \ln K_p \tag{35}$$

where the superscript e has been dropped from K_p. From here on, when K_p is used we refer to the value of the ratio given by Eq. (29) at thermodynamic equilibrium.

From the definition of the Gibbs free energy , Eq. (35) can be written:

$$\Delta H^0 - T\Delta S^0 = -RT \ln K_p \tag{36}$$

ΔH^0 and ΔS^0 represent, respectively, the enthalpy and entropy changes for reaction (28) at a pressure of one atmosphere and a temperature T. For each reaction species, the thermodynamic functions enthalpy and entropy as functions of temperature are given in the form of least squares coefficients as follows [9]:

$$\frac{H^0}{RT} = a_1 + a_2 \frac{T}{2} + a_3 \frac{T^2}{3} + a_4 \frac{T^3}{4} + a_5 \frac{T^4}{5} + a_6 \frac{1}{T} \tag{37}$$

$$\frac{S^0}{R} = a_1 \ln T + a_2 T + a_3 \frac{T^2}{2} + a_4 \frac{T^3}{3} + a_5 \frac{T^4}{4} + a_7 \tag{38}$$

where the superscript on the enthalpy H^0 and the entropy S^0 are for a reference state of one atmosphere. Usually, there is a set of coefficients for the temperature range 200 ºK to 1000 ºK and another for the range 1000 ºK to 6000 ºK. The enthalpy H^0 includes the enthalpy of formation.

3.3 Expressing the equilibrium constant in terms of moles concentrations

The equilibrium constant K_p can be expressed in a general form as:

$$K_p = \prod_{m=1}^{N} p_m^{\left(\nu_m^{"} - \nu_m^{'}\right)} \tag{39}$$

where p_m is the partial pressure of species m, N is the total number of species involved, $\nu_m^{'}$ and $\nu_m^{"}$ represent respectively, the stoichiometric coefficients of reactants and products. If the molar concentration C_m is introduced in lieu of p_m, Eq. (40) becomes:

$$K_p = \left[\prod_{m=1}^{N} C_m^{\left(\nu_m^{"} - \nu_m^{'}\right)}\right] \cdot RT^{\sum_m \left(\nu_m^{"} - \nu_m^{'}\right)} = K_C RT^{\Delta n} \tag{40}$$

$$\Delta n = \sum_{m=1}^{N} \left(\nu_m^{"} - \nu_m^{'}\right)$$

where K_C is the equilibrium constant expressed in terms of the concentration of moles. That is:

$$K_C = \prod_{m=1}^{N} C_m^{\left(\nu_m^{"} - \nu_m^{'}\right)} \tag{41}$$

In Appendix II it is shown how calculations leading to determination of equilibrium constants have been organized. The Jachimowski's reaction Nº 2, in particular, is considered.

4 VIBRATIONAL RATE EQUATION

Given a system of molecular oscillators, the differential equation that governs the rate of change of its non-equilibrium vibrational energy values is:

$$\frac{dE_v}{dt} = \frac{E_v^* - E_v}{\tau(T, \rho)} \tag{42}$$

where $E_v^*(T)$ is the vibrational energy that the system of oscillators would have if it were in equilibrium at the temperature T. The quantity τ appearing in the above equation has the dimension of time and is called the relaxation time. It is a function of the temperature and density (or pressure).

In deriving this equation, Vincenti and Kruger[10] made no assumption as to how the oscillators are distributed over the energy states when they are out of equilibrium. It can also be noted that no direct assumption has been made regarding the magnitude of the difference $(E_v^* - E_v)$. Then, the Eq. (42) should be valid even for large departure from equilibrium. Since the assumed harmonic oscillator is a valid approximation only for the lower vibrational levels, the equation is in fact limited to small departure from equilibrium. For more precise work, or for temperatures high enough that the upper vibrational states are appreciably populated, the anharmonic effects should be taken into account. The anharmonic effects in vibrational non-equilibrium were introduced as it was suggested by Wilson[5].

Despite the limitations of the harmonic oscillator, the results it gives are sufficiently accurate for most practical purposes. Furthermore it is generally assumed that Eq. (42) is valid irrespectively of the number of excited molecules and that it can be applied to in time varying environment if one takes E_v^* and τ as function of the instantaneous state of the environment. Since T and ρ (or p) are now functions of time, for the integration of Eq. (42), numerical methods must usually be used. τ is now referred to as a local relaxation time even though the process is no longer a relaxation (i.e., exponential) in strict sense.

The required explicit relation for $\tau = \tau(T, \rho)$ most commonly cited, is in the form of Landau and Teller relaxation. Precise values of the source term, however, are not important since good agreement with experimental data can, simply, be achieved assuming fast (non physical) relaxation rates [11].

In any instant or time, the total vibrational energy per unit volume

$$E_v = \sum_{j=1}^{N} E_{v_j} \tag{43}$$

is the sum of the vibrational energies for all the species which possess an internal structure. All of these species are considered to be harmonic oscillators, at a unique vibrational temperature T_v . E_{vj} for each diatomic molecule is expressed by [10]:

$$E_{v_j} = \rho_j \frac{R}{W_j} \left(\frac{\theta_{v_j}}{e^{\theta_{vj}/T_v} - 1} \right) \tag{44}$$

where θ_{vj} is the characteristic temperature for the single mode of vibration. A triatomic molecule has three vibrational modes, so its vibrational energy is written as

$$E_{v_j} = \rho_j \frac{R}{W_j} \left(\frac{\theta_{v_{j1}}}{e^{\theta_{vj1}/T_v} - 1} + \frac{\theta_{v_{j2}}}{e^{\theta_{vj2}/T_v} - 1} + \frac{\theta_{v_{j3}}}{e^{\theta_{vj3}/T_v} - 1} \right) \tag{45}$$

where there is a characteristic temperature for each of the three modes. Hydrogen peroxide (H_2O_2) has six vibrational modes, so its vibrational energy is written with six terms. Defining, after each time step, the vibrational energies like it has been made here, the total vibrational energy E_v becomes a function of only one vibrational temperature T_v. Then a Newton solver is used to find in an iterative manner that T_v.

The reaction rates so far, were presented as functions of a unique temperature. However in a flow with vibrational non-equilibrium the rates can be functions of both, translational-rotational (T) and vibrational (T_v) temperatures, respectively.

Park [12], has proposed a model in which reaction rates are a function of a geometrically averaged temperature T_a in the form:

$$T_a = T_v^q T^{1-q} \tag{46}$$

where q is between 0.3 and 0.5 for all reactions which have reactants with internal structure. With this relation, a gas with $T > T_v$ (translational energy greater than internal energy) will produce a T_a lower than T and, thus, slow the reaction rates. If $T < T_v$ (internal energy greater than translational energy), the geometrically averaged temperature would tend to speed up reactions. The vibrational energy equation has been included so that Park's model could be implemented.

5 NUMERICAL SCHEME

5.1 Extension of nonlinear scalar Total Variation Diminishing (TVD) scheme to one dimensional nonlinear systems

In this section, the method sometimes referred to as the Local Characteristic Approach in conjunction with TVD schemes is discussed. The idea of this approach is to extend the scalar TVD method to systems so that the resulting scheme is TVD for the locally frozen constant-coefficients system. The procedure relies on defining at each point a local system of characteristic variables W, and to obtain a system of uncoupled scalar equations.

Consider the hyperbolic system of equations used to describe the unsteady, quasi one-dimensional flow without source terms. Such system can be written as:

$$\frac{\partial U}{\partial t}+\frac{\partial F}{\partial U}\frac{\partial U}{\partial x}=\frac{\partial U}{\partial t}+A\frac{\partial U}{\partial x}=0 \tag{47}$$

where U is a vector with m elements and A is an m x m constant matrix with real eigenvalues. Let:

$$W=R^{-1}U \quad \text{and} \quad R^{-1}AR=\Lambda \tag{48}$$

One can then transform the above system to a diagonal form

$$\frac{\partial W}{\partial t}+\Lambda\frac{\partial W}{\partial x}=0 \qquad \Lambda=\text{diag}(a^l) \qquad l=1,...,m \tag{49}$$

Here diag (a^l) denotes a diagonal matrix with elements a^l. The matrix R is a transformation matrix such that Λ is diagonal. One then applies the nonlinear scalar scheme to each of the scalar characteristic equations.

Consider the general one-parameter family of explicit and implicit schemes of the form:

$$U_j^{n+1}+\lambda\theta\left(\widetilde{F}_{j+1/2}^{n+1}-\widetilde{F}_{j-1/2}^{n+1}\right)=U_j^n-\lambda(1-\theta)\left(\widetilde{F}_{j+1/2}^{n}-\widetilde{F}_{j-1/2}^{n}\right) \tag{50}$$

where $0\le\theta\le 1$. Obviously $\theta=0$ corresponds to an explicit scheme. The numerical flux for the second order explicit or implicit TVD schemes of Harten-Yee, can be expressed as:

$$\widetilde{F}_{j+1/2}=\frac{1}{2}\left[F_j+F_{j+1}+R_{j+\frac{1}{2}}\phi_{j+\frac{1}{2}}\right] \tag{51}$$

The matrix $R_{j+1/2}$ is R evaluated at some symmetric average U_j and U_{j+1}. For example,

$$R_{j+\frac{1}{2}}=R\left(\frac{U_{j+1}-U_j}{2}\right)$$

Other approximate way of obtaining symmetric averages is the Roe averages for a perfect gas or equilibrium real gases[13].

The elements of the vector $\phi_{j+1/2}$ for a second order upwind TVD scheme as developed by Harten and Yee are:

$$\left(\phi_{j+\frac{1}{2}}^l\right)^{SU}=\sigma\left(a_{j+\frac{1}{2}}^l\right)\left(g_{j+1}^l+g_j^l\right)-\Psi\left(a_{j+\frac{1}{2}}^l+\gamma_{j+\frac{1}{2}}^l\right)\cdot\alpha_{j+\frac{1}{2}}^l \tag{52}$$

where

$$\alpha_{j+\frac{1}{2}}^l \text{ are elements of } \alpha_{j+\frac{1}{2}}=R_{j+\frac{1}{2}}^{-1}\left(U_{j+1}-U_j\right) \tag{53}$$

$$\sigma(z)=\frac{1}{2}\left[\Psi(z)-\lambda z^2\right] \;;\; \lambda=\frac{\Delta t}{\Delta x} \;;\; \Psi(z)=|z| \tag{54}$$

$$\gamma_{j+\frac{1}{2}}^l=\sigma\left(a_{j+\frac{1}{2}}^l\right)\cdot\frac{g_{j+1}^l-g_j^l}{\alpha_{j+\frac{1}{2}}^l} \qquad \text{if} \quad \alpha_{j+\frac{1}{2}}^l\neq 0 \tag{55a}$$

$$\gamma_{j+\frac{1}{2}}^l=0 \qquad \text{if} \quad \alpha_{j+\frac{1}{2}}^l=0 \tag{55b}$$

The limiter (or amount of numerical dissipation) function g_j^l can be expressed in different ways. However, the one used here was:

$$g_j^l = min \bmod\left(\alpha^l_{j-\frac{1}{2}}, \alpha^l_{j+\frac{1}{2}}\right)$$
$$= \operatorname{sgn}\left(\alpha^l_{j-\frac{1}{2}}\right) \cdot max\left\{0, min\left[\left|\alpha^l_{j-\frac{1}{2}}\right|, \alpha^l_{j+\frac{1}{2}} \cdot \operatorname{sgn}\left(\alpha^l_{j-\frac{1}{2}}\right)\right]\right\} \tag{56}$$

Yee [1] reports that the local characteristic approach is more efficient than the exact of Godunov [14] or the approximate Riemann solvers of Osher-Solomon [15], and that it provides a natural way to linearize the implicit TVD schemes [16]. Furthermore, the limiters used in the current approach need not to be the same for each field and one can even use different schemes for different fields.

5.2 Description of an Implicit Numerical Algorithm

The finite volume approximation of the system of Eq. (51) given in this section treats only the source terms implicitly and is called a point implicit approach. The approximation can be written as:

$$\frac{\delta(UV)_j^n}{\Delta t} + \left[\widetilde{F}^n_{j+\frac{1}{2}} - \widetilde{F}^n_{j-\frac{1}{2}}\right] = (MV)_j^{n+1} \tag{57}$$

The source vector M^{n+1} is linearized using a Taylor series expansion

$$M^{n+1} = M^n + \frac{\partial M}{\partial U}\delta U^n + O\left(\Delta t^2\right) \tag{58}$$

or

$$M_j^{n+1} = M_j^n + C_j^n \delta U_j^n \tag{59}$$

where C is the Jacobian of the source term vector with respect to the conserved variables U. The calculation of this Jacobian is quite involved because of the large chemical mechanism used and because the source term may not be simple functions of the conserved variables. Following Wilson[11] define a functional form of the source term vector as:

$$M(U) = M\left[U, T(U)\right] \tag{60}$$

so that C can be written with the chain rule as:

$$C = \frac{\partial M}{\partial U} + \frac{\partial M}{\partial T}\frac{\partial T}{\partial U} \tag{61}$$

To separate the combined rate of change in both U and V so that δU^n may be solved directly, it is written:

$$\delta(UV)^n = V^{n+1}\delta U^n + U^n \delta V^n \tag{62}$$

The result of substituting Eqs. (59),(61) and (62), into Eq. (57) is:

$$\left(I - \Delta t C_j^n\right)\delta U_j^n = \Delta U_j^n + \Delta t M_j^n \tag{63}$$

where ΔU_j^n represents the explicit right hand side (RHS) terms which are:

$$\Delta U_j^n = -\frac{\Delta t}{V_j^{n+1}}\left[U_j^n \frac{\delta V_j^n}{\Delta t} + \widetilde{F}_{j+\frac{1}{2}}^n - \widetilde{F}_{j-\frac{1}{2}}^n\right] + \Delta t M_j^n \tag{64}$$

The updated solution at the new time level n+1 is then

$$U_j^{n+1} = U_j^n + \delta U_j^n \tag{65}$$

Leveque and Yee [17] have stated that achieving second-order accuracy in time with an implicit treatment of source terms as described previously, requires the following form:

$$\left(I - \frac{1}{2}\Delta t C_j^n\right)\delta\overline{U}^n = \Delta U_j^n + \Delta t M_j^n \tag{66}$$

$$\overline{U}_j^n = U_j^n + \delta\overline{U}_j^n$$

and the corrector step is:

$$\left(I - \frac{1}{2}\Delta t C_j^n\right)\delta\widetilde{U}^n = \Delta\overline{U}_j^n + \Delta t M_j^n \tag{67}$$

$$U_j^{n+1} = U_j^n + \frac{1}{2}\left(\delta\overline{U}_j^n + \delta\widetilde{U}_j^n\right)$$

In this scheme the terms involving the source terms (C_j^n and M_j^n) are evaluated using U_j^n on both the predictor and corrector steps, and a factor 1/2 in the source term Jacobians.

5.3 About the contact discontinuity

Because there is no mass flux across the contact discontinuity, the flux vector can be written:

$$\bar{F} = \left(0,...,0, p^c, 0, u^c p^c\right) \tag{68}$$

where p^c and u^c are the local static pressure and the local fluid velocity respectively, both being evaluated by the Riemann solver proposed by Jacobs[3]. By way of tracking the discontinuity, the issue of smearing gas interfaces by numerical diffusion is completely avoided. Furthermore, this approach is particularly well suited to one-dimensional problems. Not all of the improvement from the interface tracking is due to the removal of numerical diffusion; a side benefit is that it provides an easy way to concentrate grid points where they are needed.

6 RESULTS

6.1 Expansion Tube Application

The NASA-GASL HYPULSE expansion tube (Fig. 1), is composed of three sections: a driver (2.44m long and 16.51cm diameter), an intermediate section (7.49m long and 15.24cm diameter), and the acceleration section (14.62m long and 15.24cm diameter). The test gas is contained in the intermediate section [18].

The operation of the expansion tube begins by rupturing a thick diaphragm separating high-pressure helium used as driver gas, from the test gas. A right-traveling shock wave (primary shock) is produced which travels into the test gas. At the end of the intermediate tube a thin second diaphragm is encountered and is ruptured. This creates a second incident shock (secondary shock) and an expansion both of which travel down the acceleration tube. The unsteady expansion of the test gas creates the high velocity test conditions. It is said that the expansion tube operates ideally when the secondary diaphragm is removed instantaneously upon arrival of the primary incident shock. However, it does not happen in this way since regardless of the type of diaphragm, it takes time to break and clear the flow area. To approximately account for this opening

time, it is usually assumed that the secondary diaphragm remains rigid for a prescribed short amount of time, and there after is instantaneously removed.

For the Mach 17 HYPULSE test condition considered here, the driver section was filled with helium and the reported pressure and temperature were 37.9 MPa and 380 ºK respectively. The intermediate section pressure was initially at 3.43 kPa , and the acceleration section pressure was 7.2 Pa, being both sections filled with air at 292ºK. Fig. 2 contains a computed *x-t* diagram of the logarithm of constant density lines for the flow within the expansion tube, with an assumed 25 microseconds delay of the secondary diaphragm. In addition to the known features, which in the flow within an ideal expansion tube can be found, the enlargement of the secondary diaphragm region depicts the incident shock reflected by the secondary diaphragm before rupturing. Although the reflected shock is quickly weakened by the rarefaction produced after the diaphragm is removed, it is still able to cause a significant disturbance after reflecting off the primary interface. Shinn and Miller[19] have reported this kind of interaction.

A peculiar feature of the expansion tube among other types of pulse facilities is that in its ideal operating sequence, no regions of stagnant flow inside the facility are created, and therefore, high temperatures to dissociate the test gas are avoided. If this can be done, a better simulation of the free stream conditions seen by a high-speed vehicle can be achieved. However, when the primary shock reflects off the secondary diaphragm as shown in Fig. 2, a small stagnant region of hot gas in the intermediate tube is created. This will produce dissociation of the test gas, which could affect the quality of the flow. The finite rate chemistry coupled with the fluid dynamic part of the code allows the estimation of the amount of dissociation that originates behind the reflected primary shock, and determine if they persist until the test region or full recombination occurs before.

Fig. 3 shows traces of O mass fractions from the simulation. The large quantity of monatomic oxygen behind the secondary shock is caused by the very high temperature that reaches de acceleration gas. The region of the test gas is behind de secondary interface and so is labeled in the figure. For the ideal case is little dissociation as expected, however, for the 25 microsecond opening time there is a significant amount of dissociation in the test gas. The computed traces of NO mass fractions (Fig. 4) show that this molecule is present in significant amounts as well.

Higher mass fractions of dissociated species in the test flow originate from high temperatures behind the reflected primary shock. These higher mass fractions persist until the test region because the secondary expansion freezes the chemical composition before full recombination can occur. It can be inferred from the simulation that the area affected by a reflected shock does not have to be large to significantly alter the test conditions that, supposedly, should be provided by the facility.

The calculations to which reference is made here were performed with a mesh of 500 points along the tube axis and with 5000 time steps. Nearly identical results were obtained with 1000 grid points. Solution times for the 500 point mesh and 5000 time steps were approximately 80 minutes on a Pentium II PC with 64 MB of RAM.

6.2 Shock Tube Application

As it was said in the previous introduction, the conversion of Hypulse into a shock tube can be accomplished simply installing a thick secondary diaphragm. The primary shock reflects from this diaphragm and a stagnant flow region with high pressure and temperature, is created. If such region is to be used as the plenum of a shock tunnel, pressure and temperature shall remain quasi-steady the longest possible time. For given lengths of the driver and of the driven, the longest running time of the facility is obtained if the reflected primary shock goes right trough the contact discontinuity without reflecting waves. When this happens, it is said that the shock tube is operating in a tailored mode. There is interest in knowing if, in spite of considering real gases, calculations can still predict the tailored mode.

The computed x-t diagram of temperature contours shown in Fig. 5, indicates that a tailored interaction between the reflected shock and the contact discontinuity has been produced. Helium heated to 810 ºK and with an initial pressure of 37.9 MPa was the driver gas, and the driven gas was air at 292 ºK and the initial pressure 120.3 kPa. A temperature trace taken across the region of test gas 5.5 milliseconds after diaphragm rupture, is presented in Fig. 6. It shows that the temperature remains almost constant in the region of test gas. Fig 7 shows that NO is also present in that region, however, its concentration approximates the value

obtained with equilibrium calculations, thus indicating that the high pressure behind the reflected shock brings the gas to equilibrium almost immediately.

7 CONCLUSION

A technique for numerically simulating quasi one-dimensional flows has been presented. The numerical formulation solves, simultaneously, the unsteady Euler equations and 13 species equations with coupled finite rate chemistry. An implicit finite-volume upwind TVD scheme, a Riemann solver for tracking interfaces and a moving mesh, have been included to overcome numerical difficulties associated with high energy flows (e.g. capture of shock waves, smearing of gas interfaces by numerical diffusion and concentration of grid points where they are needed). The potential of the current numerical approach has been demonstrated by computing the flow in two different applications. In the first, the effects of the finite opening time of the secondary diaphragm on the chemical composition of Hypulse's test flow, has been investigated. In the second, the simulation of a tailored operating helium driven shock tube taking into account real gas effects, has been made.

Acknowledgments. The authors would like to acknowledge and thank the support of the Secretary of Science and Technology of the National University of Córdoba, and the cooperation of the Applied Research Center of the Aeronautical University Institute. A fellowship granted by the FONCYT, has made possible the third author's participation in this project.

REFERENCES

[1] YEE, H., A class of high-resolution explicit and implicit shock capturing methods, *NASA TM 101088*, 1989.

[2] JACOBS, P., Single-block Navier-Stokes integrator, *NASA Contract Not. NAS1-18605*, 1991.

[3] JACOB, P.A., Approximate Riemman Solver for hypervelocity flows. AIAA Journal, Vol.30, Nº10, 1992.

[4] JACHIMOWSKI, C.J., An analytical study of the Hydrogen-Air reaction mechanism with application to Scramjet combustion. NASA TP2791, Feb.1988.

[5] WILSON, G., Time-dependent quasi-one-dimensional simulations of high enthalpy pulse facilities, *AIAA Paper–92-5096*, 1992.

[6] JANAF *Thermochemical Tables, Journal of Chemistry Reference Dates*, Vol 14, Supl. 1, 1985.

[7] PENNER,S.S., "Chemistry problems in Jet Propulsion", Pergamon Press, New York, 1957. Library of Congress Card No. 57-14445, USA.

[8] WILLIAMS, F.A., "Combustion Theory", 1st Ed., Addison-Wesley Publishing Company, Inc., Reading, Massachusetts, 1965. Library of Congress Catalog Card No. 64-16915, USA.

[9] GORDON, S., McBRIDE, B. J., Calculation of Complex Chemical Equilibrium Compositions, Rocket Performance, Incident and Reflected Shocks, and Chapman-Jouguet Detonations, NASA SP-273, March 1976.

[10] VINCENTI, W. G., KRUGER, CH. H., "Introduction to Physical Gas Dynamics", John Wiley and Sons, Inc., New York, 1965. Library of Congress, Catalog Card No. 65-24297, USA.

[11] WILSON, G. J., "Computation of unsteady shock-induced combustion over hypervelocity blunt bodies", Ph.D Tesis, Stanford University, 1992.

[12] PARK; C., Assessment of Two-Temperature Kinetic Model for Dissociating and Weakly-Ionizing Nitrogen, Journal of Thermophysics and Heat Transfer, Vol 2, pp. 8-16,1988.

[13] ROE, P. L., Approximate Riemann Solvers, Parameter Vectors and Difference Schemes, J. Comp. Phys., Vol 43, pp. 357-372, 1981

[14] GUDONOV, S. K., A Finite Difference Method for the Numerical Computation of Discontinuous Solution of the Eq. of Fluid Dynamics, Mat. Sb. 47, pp. 357-393, 1959.

[15] OSHER, S., SOLOMON, F., Upwind Schemes for Hyperbolic Systems of Conservation Laws, Math. Comp., Vol. 38, pp. 339-377, 1987.

[16] YEE, H. C., Construction of Explicit and Implicit Symmetric TVD Schemes and their Applications, J. Comp. Phys., Vol 68, pp. 151-179, 1987; also NASA TM-86775, July 1985.

[17] LEVEQUE, R. J., YEE, H. C., A study of Numerical Methods for Hyperbolic Conservation Laws with Stiff Source Terms, J. of Comp. Physics, 86, 187-210, 1990.

[18] TAMAGNO, J., BAKOS, R., PULSONETTI, M. and ERDOS, J., Hypervelocity real gas capabilities of GASL's expansion tube (HYPULSE) facility. *AIAA Paper 90-1390*, 1990.

[19] SHINN J. and MILLER C., Experimental perfect gas study of expansion tube flow characteristics. *NASA TP 1317*, 1978.

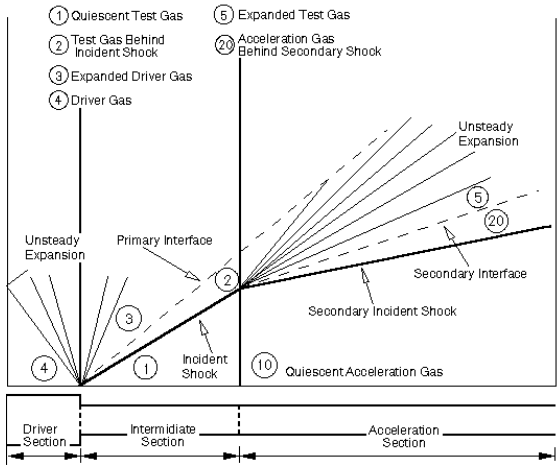

Figure 1 – Expansion tube scheme.

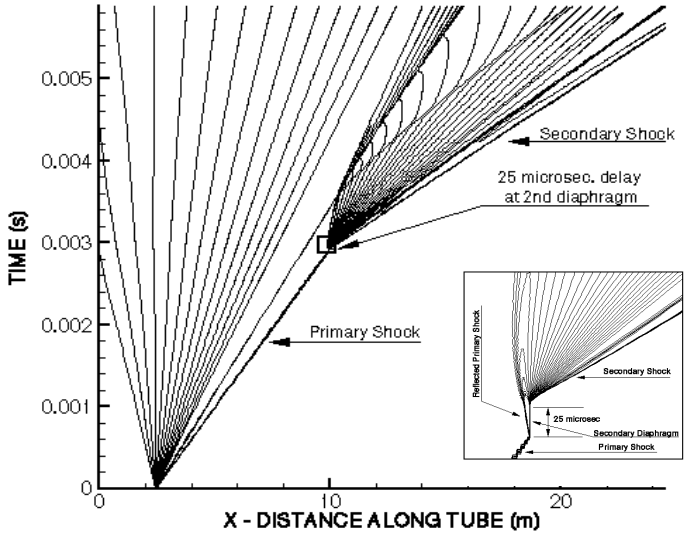

Figure 2 – Computed X-T Diagram of Logarithm of Density Contours. Mach 17 HYPULSE test condition.

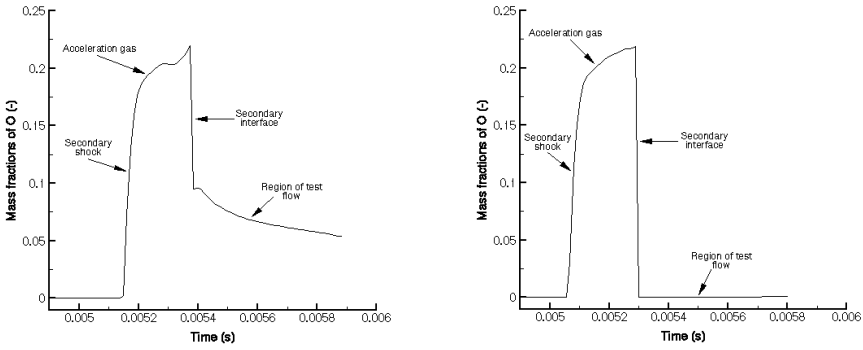

Figure 3 - Computed mass fractions of atomic Oxygen at X=22m – The left figure corresponds to the 25 microsec delay case at the secondary diaphragm and the right figure corresponds to the no delay case.

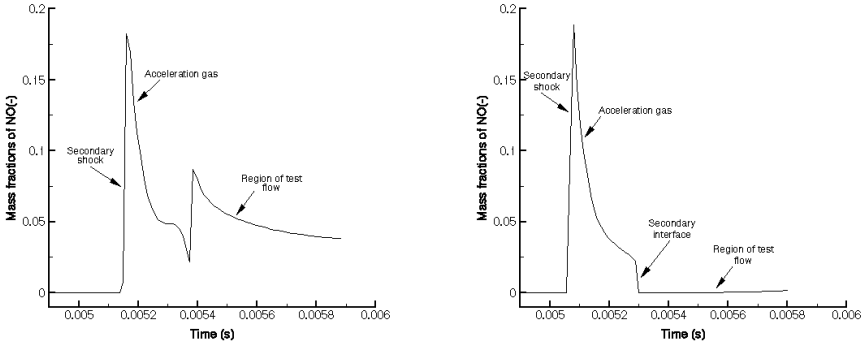

Figure 4 - Computed mass fractions of NO at X=22m – The left figure corresponds to the case of 25 microsec. delay at the secondary diaphragm and the right figure corresponds to the case of no delay.

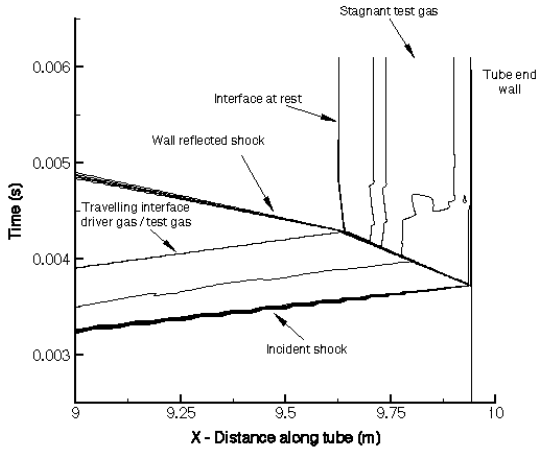

Figures 5 – Computed temperature contours. Tailored interface operating mode of reflected shock Tube.

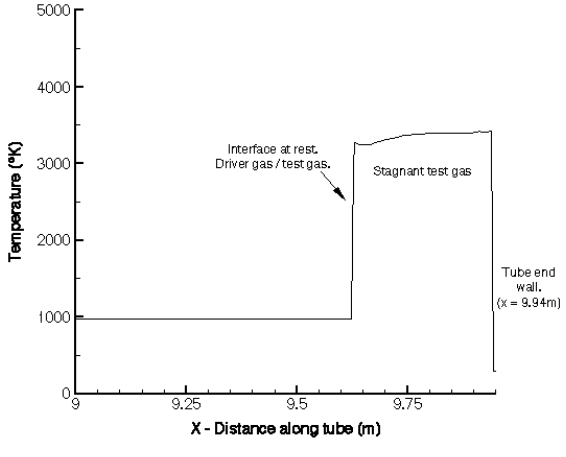

Figure 6 - Computed temperature distribution along tube at 5.5 milliseconds after the rupture of the primary diaphragm. Tailored interface operating mode of a reflected shock tube.

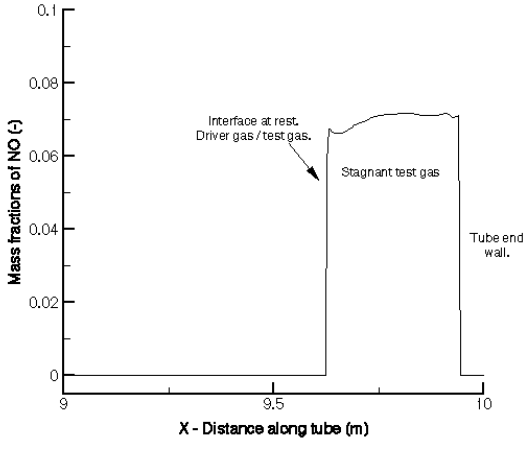

Figure 7– Computed mass fractions of NO along tube at 5.5 milliseconds after the rupturing of the primary diaphragm. Tailored interface operating mode of a reflected shock tube.